Morphological and chemical evolution of monocrystalline porous germanium over time in various storage environments

Valentin Daniel, Jérémie Chretien, Sonia Blais, Jinyoun Cho, Kristof Dessein, Gwenaelle Hamon, Abderraouf Boucherif, Maxime Darnon

MNE 24 (2024) 100274

Contents lists available at ScienceDirect

Micro and Nano Engineering

journal homepage: www.sciencedirect.com/journal/micro-and-nano-engineering

Morphological and chemical evolution of monocrystalline porous germanium over time in various storage environments

Valentin Daniel [a,b,*], Jérémie Chretien [a,b], Sonia Blais [c], Jinyoun Cho [d], Kristof Dessein [d], Gwenaelle Hamon [a,b], Abderraouf Boucherif [a,b], Maxime Darnon [a,b]

[a] Institut Interdisciplinaire d'Innovation Technologique (3IT), Université de Sherbrooke, 3000 boulevard de l'Université, Sherbrooke J1K 0A5, Québec, Canada
[b] Laboratoire Nanotechnologies Nanosystèmes (LN2) - CNRS IRL-3463 Institut Interdisciplinaire d'Innovation Technologique (3IT), Université de Sherbrooke, 3000 boulevard de l'Université, Sherbrooke J1K 0A5, Québec, Canada
[c] Centre de Caractérisation des Matériaux (CCM), Université de Sherbrooke, 2500 Boul. Université, Sherbrooke J1K 2R1, Canada
[d] Umicore Electro-Optic Materials, Watertorenstraat 33, 2250 Olen, Belgium

ARTICLE INFO

Keywords:
Electrochemical etching
Mesoporous germanium
Aging
Oxidation
Shelf life

ABSTRACT

Mesoporous germanium (MP-Ge) emerges as a very appealing material for many applications such as anode material for Lithium-Ion batteries due to it high specific area and large void spaces or, in optoelectronics as sacrificial layer for III-V materials growth and detachment, allowing notably several uses of a single Ge substrate. These porous nanostructures are distinguished by a large specific surface area and are prone to degradation with time due to exposure to the environment. To understand and be able to reduce this effect, we studied the chemical and morphological evolution of porous germanium layers under various ambient storage conditions for 3 months to identify the main parameters responsible for material degradation. This study demonstrates that the ambient air environment leads to the growth of native oxide, leading to major morphology changes. Scanning electrons microscope (SEM) showed the formation of clusters and the enlargement of the pores after 90 days. These structural modifications are caused by the oxidation of Ge, and more specifically by the creation of GeO_2 matrices due to the synergy of dioxygen (O_2) and humidity ($H_2O_{(g)}$). The energy brought by light can exacerbate these phenomena and thus accelerate the degradation rate of the pore morphology. Based on these experimental results, we propose efficient solutions to limit the GeO_2 proportions and the clusters' appearance, by storing them under a dry neutral atmosphere (Ar) or by adding a hydrogen halide pre-treatment (10s 1% HBr solution).

1. Introduction

Germanium (Ge) is a group IV semiconductor that has applications for microelectronic devices [1], optoelectronic applications in the near-infrared region [2], and as a substrate for crystalline III-V compound semiconductor growth [3,4] Conserving its quality over time is thus a crucial parameter to improve the lifespan of technologies using this type of material and to facilitate its processing. Due to interesting characteristics such as its large spectral transparency range, its high specific surface, its tunable refractive index and its biocompatibility, the nanostructuring of germanium has been developed for various applications such as energy storage [5] or optoelectronic devices [6,7], using different techniques [8–12] to configure its optical [13], morphological, or mechanical properties. In the specific case of monocrystalline porous germanium made by bipolar electrochemical etching for epitaxy of group IV and III-V materials [7,14,15], the preservation of the structural integrity (composition, porosity morphology, and surface roughness) of the material is an essential criterion for high-quality epitaxial growth. For this purpose, we propose in this study to observe the evolution of monocrystalline mesoporous germanium over time in ambient air (in a box in a clean room) and other specific conditions, to characterize the aging of the material, to analyze the origin of potential deteriorations, and to propose adequate storage conditions to maximize the shelf-life of a nanostructured germanium layer.

2. Methods

2.1. Porous germanium sample preparation

For our investigations, a mesoporous structure is created on a 4″

* Corresponding author.
E-mail address: valentin.daniel@usherbrooke.ca (V. Daniel).

https://doi.org/10.1016/j.mne.2024.100274
Received 7 December 2023; Received in revised form 8 March 2024; Accepted 15 July 2024
Available online 20 July 2024

monocrystalline p-type (100) oriented germanium wafer with 6° miscut toward (111) crystallographic direction by a bipolar-electrochemical etching. This nano-structuration technique uses alternately positives and negatives electrical pulses in an acid solution (HF). The additional advantage of this procedure is that it leaves the surface almost oxide-free due to the acid etch and the temporary passivation of the surface by F^-. The porosification process used has been developed as a part of previous research [14] for detachable III-V germanium-based photovoltaic cells. The 250 nm-thick "sponge-like" porous layer (Ge_{porous} layer) created is uniform and monocrystalline with a porosity of 51% ± 5% (estimated by image treatment). After porosification, the 4" Ge wafer is then cleaved into five 5 × 5 mm^2 samples to facilitate the storage and parallelize aging processes on originally similar samples.

2.2. Storage conditions

Each porous sample is stored individually for up to 90 days. In the first case, some of them are placed in semi-transparent boxes exposed to light under class 100 clean room ambient conditions (humidity = 43% ± 5%, temperature = 19.5 °C ± 2 °C). For experiments in controlled storage conditions, we developed a packaging process using hermetic metallic bags (Fig. 1) prepared in a glove box containing a neutral atmosphere: Argon (Ar). A preliminary study carried out with Nitrogen (N_2) demonstrated the same behaviour as Argon, indicating that both gases can be used as a neutral atmosphere for the storage. The samples are placed in individual boxes and sealed in hermetic bags either with wet tissue (*dark moist Ar*) or dry silicate beads (*dark dry Ar*). These storage containers can then be theoretically exposed to the ambient atmosphere with no contamination by the external environment. This encapsulation technique is validated by experiment results shown further (**part 4.1**).

For conditions with O_2, the samples are placed in non-hermetic black boxes exposed to the clean room air with *dark dry* O_2) or without silica beads (*dark moist* O_2). When the light impact is considered, the metallic bag is not used, and the sample is placed in an illuminated part of the cleanroom in a transparent box (*light moist* O_2). For all dry conditions (see Table 1), humidity testers are also placed in the storage area to prove the enclosure has remained dry throughout the entire study and we verified that the humidity never exceeded 10% in dry conditions.

2.3. Characterizations

Samples are analyzed after 2 h from porosification (initial condition – reference), 1, 7, 30, and 90 days of aging (one sample per aging duration for each condition). To characterize the evolutions in composition and the morphological transformation of the Ge_{porous} layer, we used X-ray Photoelectron Spectroscopy (XPS) with an Al kα 15 kV (225 W, 15 mA) monochromatic excitation source as well as Scanning Electron Microscopy (SEM) at 20 kV with a 150,000× magnification and a working distance (WD) of 5.5 mm ± 1 mm, for cross-sectional and top views observations. For the XPS spectrum analysis, we set the C*1s* core level spectrum with sp^3 (adventitious carbon) component peak at 284.8 eV (Thermo Fisher database). Then, on the Ge*3d* core level spectrum

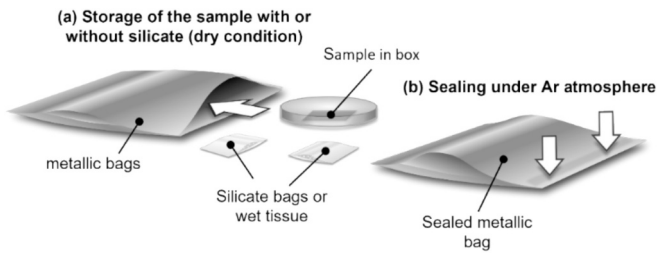

Fig. 1. Schematic illustration of the sealing process used for controlled dark moist and dry Argon storage environment.

Table 1
Summarizes the storage conditions.

Name	Objective	Storage condition
Clean room	Normal storage (reference)	Semitransparent box in cleanroom environment (humidity = 43% ± 5%, temperature = 19.5 °C ± 2 °C).
Dark dry Ar	Inert storage	Metallic bag sealed in an Argon-filled glove box. Silica beads. Humidity tester below 10%
Dark dry O_2	Impact of O_2	Non-hermetic black box exposed to air with silica beads
Dark moist Ar	Impact of water vapor	Metallic bag sealed in an Argon-filled glove box with a wet tissue.
Dark moist O_2	Synergetic impact of water vapor and O_2	Unsealed metallic bag in a cleanroom environment (humidity = 43% ± 5%, temperature = 19.5 °C ± 2 °C).
Light moist O_2	Role of light	Transparent box cleanroom environment (humidity = 43% ± 5%, temperature = 19.5 °C ± 2 °C).

region, the Ge^0 components ($Ge3d^{5/2}$ and $Ge3d^{3/2}$) are curve fit with the same full width at half maximum (FWHM), with a 2/3 intensity ratio and a shift of 0.58 eV [16,17]. These parameters allow determining the precise position of the germanium oxidation states 3d peaks, Ge^{1+} (related to the Ge_2O suboxide), Ge^{2+} (related to the GeO suboxide), Ge^{3+} (related to the Ge_2O_3 suboxide), and Ge^{4+} (related to the GeO_2 oxide) shifted from the Ge^0 position (calculated for the first case at 29.5 eV) by 0.8 eV, 1.8 eV, 2.75 eV and 3.4 eV, respectively [13,14]. One of their possible configurations is schematically represented in Fig. 2. The peaks are fitted by a Gaussian/Lorentzian function after subtracting a baseline using a Shirley function. The resulting fitting curve enables to extract of the proportion of each oxide species by considering the instrument transmission function. The surface roughness is eventually determined using tapping mode on 5 × 5 μm wide areas using atomic force microscopy (AFM).

3. Aging of porous Ge in clean room conditions

The SEM images comparison (Fig. 3 **(a-d)**) between the reference sample (as porosified after 2 h of aging) and the one aged during 3 months shows an important difference in their morphology (visible deterioration over time). The sample after 90 days has larger pores and seems to present clusters. The XPS survey spectrum (Fig. 3 **(e)**) shows major differences in the composition after 90 days, notably with the appearance of oxygen in the porous germanium structure observable via an increase of the Auger OKLL lines and O*1s* peaks and by modifications of the Ge-related peaks (GeLMM, Ge2p, and Ge3d). Coherently with the literature [16–20], we can identify on the Ge*3d* peak (Fig. 3 **(f)**, the contribution from different germanium oxide and suboxide species: Ge_2O (Ge^{1+}), GeO (Ge^{2+}), Ge_2O_3 (Ge^{3+}), and GeO_2 (Ge^{4+}).

When we look at the kinetic evolution of the Ge*3d* peak by XPS (Fig. 4), we observe initially the formation of Ge_2O quasi instantly after porosification (initial proportions around 17% after 2 h – reference). After 1 day of aging, Ge_2O increases up to ~18% and other suboxides such as the GeO and Ge_2O_3 appear, both with proportions around 10%. Ge_2O and GeO chemical contributions then decrease, while Ge_2O_3 continues to increase until one week of aging. At the same time, we begin to observe the creation of GeO_2 oxide (below 20% before the first 7 days of storage). All the suboxides then gradually give way to the formation of GeO_2 up to 60% after the first month of storage. This final oxide analogous to the Ge^{4+} germanium oxidation state keeps slightly increasing afterward. These observations indicate an evolution of the germanium oxidation state from Ge^{1+} (Ge_2O) and Ge^{2+} (GeO) to Ge^{3+} (Ge_2O_3) and finally to Ge^{4+} (GeO_2). After 90 days, the GeO_2 oxide corresponds to approximately 65% of the Ge3d peak. The morphological modification of the porous germanium starts to be observed between 1 and 7 days of storage in clean room conditions (hatched zone in the

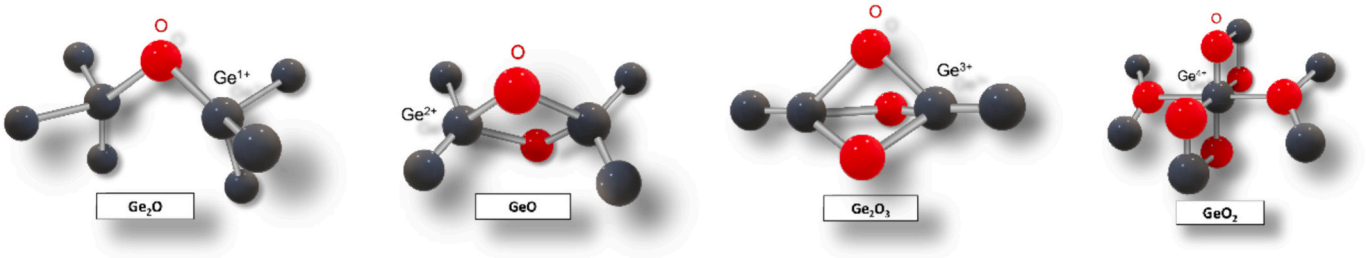

Fig. 2. Schematic representation of a possible configuration of Ge^{1+}, Ge^{2+}, Ge^{3+} and Ge^{4+}.

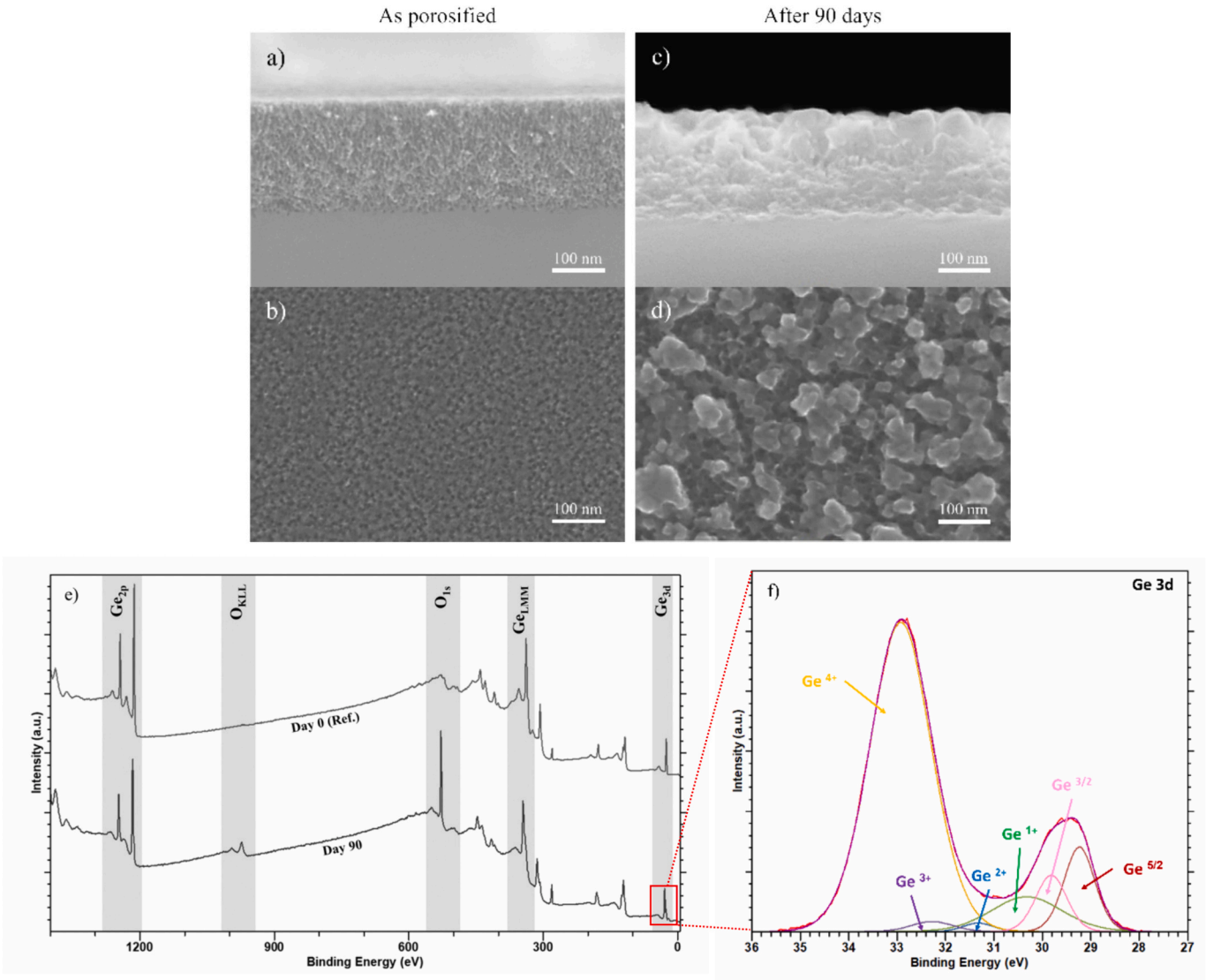

Fig. 3. a) Cross-section SEM, b) top-view SEM images of the "as porosified" germanium sample (initial conditions - reference) compared to c) Cross-section SEM and d) top-view SEM images of the same sample after 90 days of storage under clean room conditions. e) XPS survey spectrum with the main modified element peaks of Ge_{porous} "as porosified" compared to the same sample after storage, and f) zoom on the Ge_{3d} area detailing the different Ge (I-IV) oxidation states.

graph Fig. 4).

Based on these first results, we can postulate germanium quickly ages in clean room conditions (modification of the porosity and appearance of cluster) and that the oxidation of the germanium porous structure is responsible for its structural transformation. However, these preliminary observations are not sufficient to determine the precise mechanism of this degradation and to identify the contribution of each environmental parameter to the morphological deterioration over time. We characterized then, separately and combined, the impact of ambient components presents during the storage of the samples and potentially responsible for the Ge_{porous} evolution: dioxygen (O_2), humidity, and light.

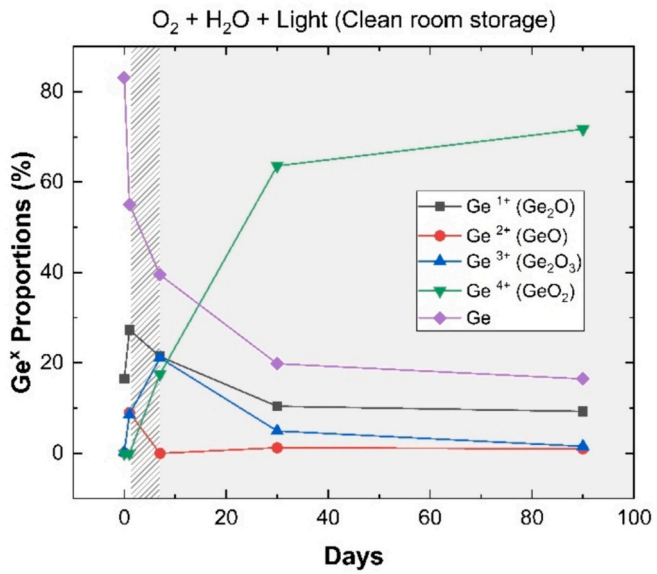

Fig. 4. Ge oxides proportions evolution during 90 days under conventional clean room environment. The gray background indicates a degraded morphology (observed by SEM) while the hatched background delimitates the period when the porous layer begins to morphologically evolve.

4. Impact of storage environmental condition on porous germanium aging

4.1. Validation of the storage protocol

The chemical composition (Fig. 5) and the morphological aspect (Fig. 6) of the samples stored in Ar after 90 days are comparable to the "as porosified" sample (reference – Fig. 3 **(a-b)**). We notice a limitation of the native suboxides quantity, mostly dominated by Ge_2O (proportions variation from 17% initially to ~30% after 3 months in Ar), over time. The Ge_{porous} structure shows no visible structural modification (same porosity ~50% and no cluster formation). This comparison underlines that this storage process under a neutral atmosphere preserves the sample from external oxidation (by air dioxygen or humidity), and thus can be used for controlling the sample environment during this aging study.

4.2. Influence of dioxygen (O_2)

In this first case, we focused on the ambient dioxygen influence on the Ge_{porous} structure by comparing *dark dry Ar* and *dark dry* O_2 conditions.

4.2.1. Kinetic of germanium oxide and sub-oxides evolution

We compare here the proportions of different germanium oxidation states in the G*3d* peak over time, represented in Fig. 5. Under *dark dry Ar* storage (Fig. 5 **(a)**), we observe a small evolution of Ge_{porous} chemical composition. We only notice low oxidation states, associated with the formation of native suboxides Ge_2O (Ge^{1+}) and GeO (Ge^{2+}). Between the first week and the end of the study, the proportions of germanium are constant, and we only observe modifications in the oxidation states (notably Ge^{2+} turning progressively into Ge^{1+}). After 90 days, these samples aged in neutral conditions solely show the presence of Ge_2O suboxide (~30%). In comparison, under *dark dry* O_2 storage, we notice higher oxidation states. Such as in *clean room* storage conditions, we notice at first the creation of Ge^{1+}, Ge^{2+}, and Ge^{3+} after one day of aging. Then, beyond the first week of oxidation, we see a decrease in the proportions of the GeO (Ge^{2+}) and a slow reduction of the Ge_2O (Ge^{1+}) amount. In parallel, an increase followed by a stabilization of the Ge_2O_3 (Ge^{3+}) quantity can be noticed after one month. At the end of the aging process (90 days), only Ge^{1+} (25%), Ge^{3+} (22%) suboxides, and few Ge^{4+} (4%) oxides are detected. These data demonstrate that a *dark dry Ar* environment significantly decreases the quantity of germanium suboxides formed compared to storage under *dark dry* O_2 and that storage in *dark dry* O_2 does not induce a significant formation of GeO_2 (Ge^{4+}).

4.2.2. Morphological evolution after 90 days of storage

Concerning the morphology, despite a high proportion of suboxides, we do not see any evolution in the Ge_{porous} structure. As shown in Fig. 6 **(a-d)** and Fig. 6 **(e-h)**, respectively in both environmental conditions, the morphology, the porosity, the thickness, and the surface roughness did not change even after 3 months of storage. Thus, ambient O_2 gas does not appear to be solely responsible for the porous Ge structural transformation (observable under *clean room* conditions), and the formation of suboxides (GeO_x with $x < 2$) is not the cause of oxide cluster formation.

4.3. Influence of humidity (moist conditions)

We study in this part the consequences of the presence of humidity in an inert gas (*dark moist Ar*) combined with ambient dioxygen (*dark moist* O_2), inside the dark enclosure in both cases. These observations allow us

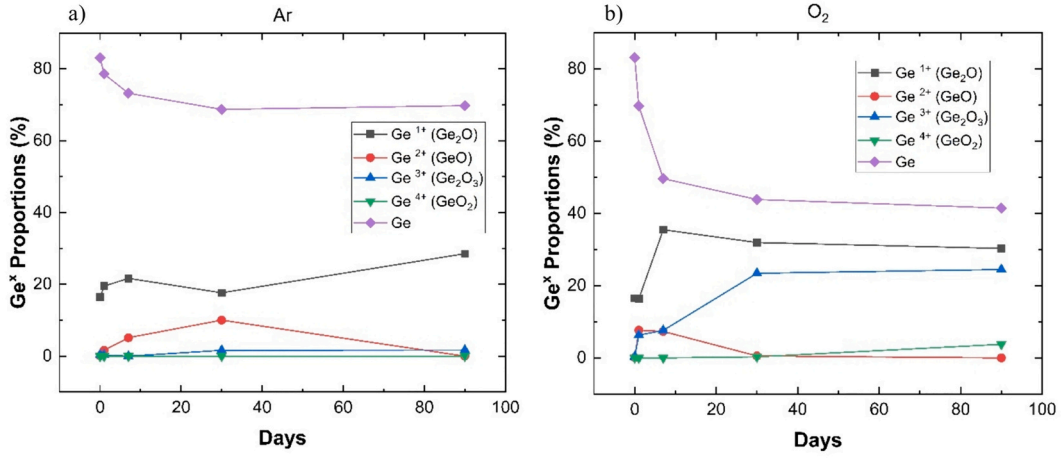

Fig. 5. Proportions of Ge oxides evolution during 90 days under a) dark dry Ar and b) dark dry O_2 storage conditions.

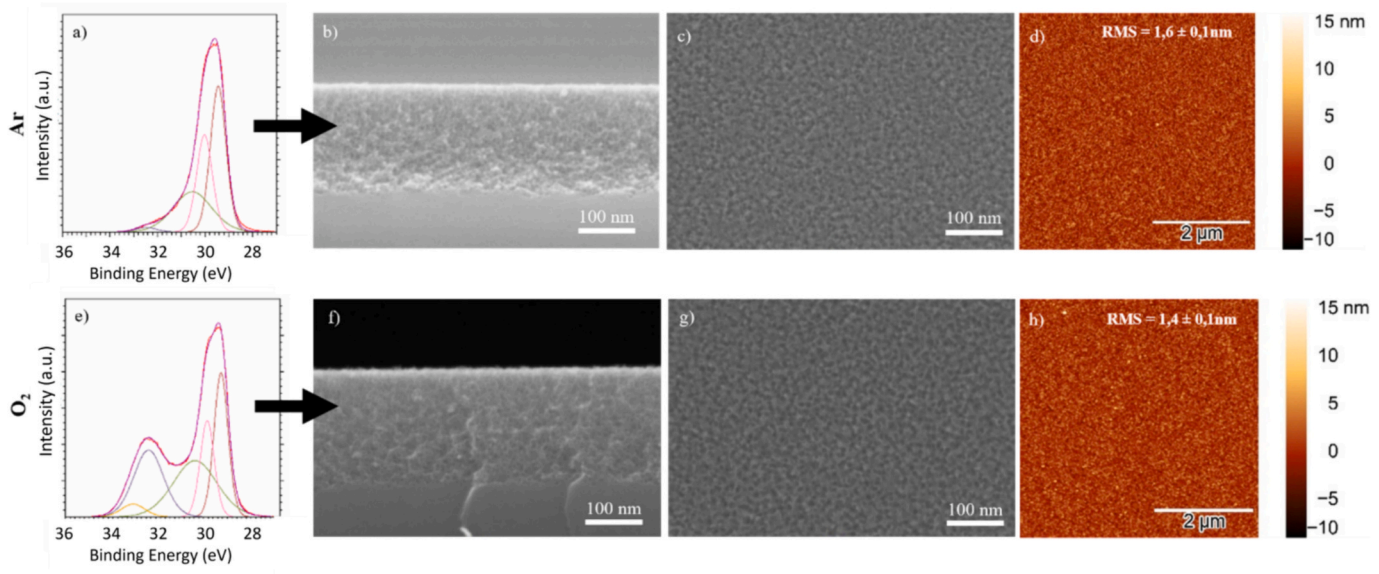

Fig. 6. a) XPS Ge3d spectrum, b) cross-section SEM images, c) Top SEM view and d) 5 × 5um surface roughness made by AFM of porous germanium stored in dry Ar after 3 months of storage. e) XPS Ge3d spectrum, f) cross-section SEM images, g) Top SEM view and h) 5 × 5um surface roughness made by AFM of porous germanium stored in dry O_2, after 3 months of storage.

to identify the impact of humidity in the storage conditions and its contribution to the structural modification of the porous germanium layer over time.

4.3.1. *Kinetic: germanium oxide and sub-oxides evolution*

In the presence of humidity in a neutral atmosphere (*dark moist Ar*) as shown in Fig. 7 **(a)**, we can distinguish the same oxides and suboxide evolutions as for the sample stored in a dry dioxygen environment (*dark dry O_2* Fig. 5 **(b)**), but slightly slower: initial formation of Ge_2O (Ge^{1+}) (proportions around 17%), followed by the germanium oxidation state Ge^{2+} and Ge^{3+} associated to the GeO and Ge_2O_3 formation respectively. We notice the formation of a few quantities of GeO_2 (related to the Ge^{4+} oxidation state) after several weeks of aging (1.4% after 90 days). When the humidity is combined with the O_2 in the storage conditions (*dark moist O_2*, Fig. 7 **(b)**), we can observe an oxidation synergy and the creation of a high quantity of GeO_2 after the first week of aging. This massive formation of Ge^{4+} oxidation states (45% after 90 days) is associated with a decrease in the suboxides proportion. With Fig. 7 **(b)**, we can thus deduce that the germanium and its low oxidation states evolve gradually into GeO_2 over time when O_2 is associated with humidity.

4.3.2. *Morphological evolution after 90 days of storage*

When we focus on the morphological transformations of the Ge_{porous} layer stored with humidity in a neutral atmosphere (*dark moist Ar*, Fig. 8 **(a-d)**), we do not observe important structural changes (same morphology compared to the reference), even if XPS reveals the presence of suboxides (GeO_x with $x < 2$), similar to *dark dry O_2* storage conditions (Fig. 6 **(e-h)**).

In the case of the sample stored under an O_2 and H_2O environment (*dark moist O_2*) in Fig. 8 **(e-h)**, we observe the degradation of Ge_{porous} structure with the creation of oxide matrices (clusters), an increase of the porosity (84% ± 5%) and a higher surface roughness (4.8 ± 0.5 nm). This transformation begins between 7 and 30 days of storage under these oxidative conditions. Combined with the XPS characterization, we can correlate the formation of a large amount of Ge^{4+} (GeO_2) with this appearance of clusters and the pore size expansion. This morphological evolution over time can be explained by the combination of the Ge

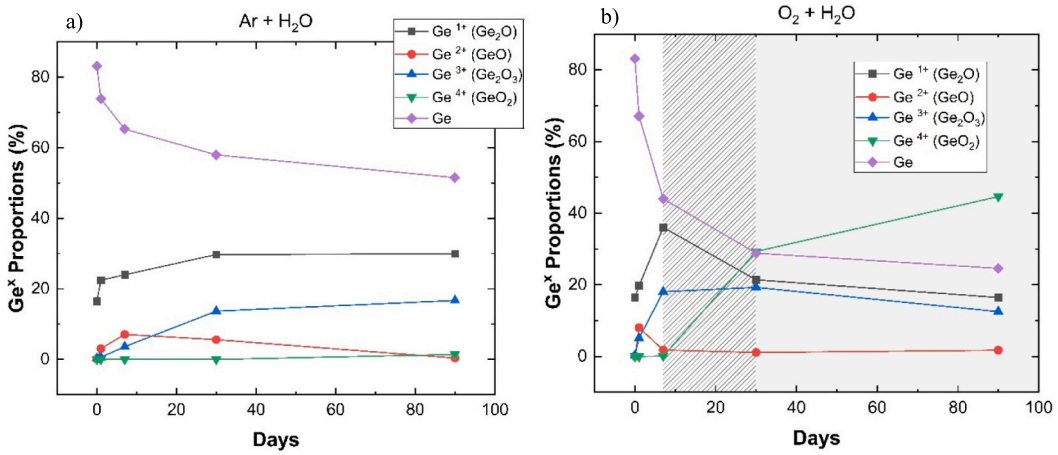

Fig. 7. Proportions of Ge oxides evolution during 90 days under a) dark moist Ar and b) dark moist O_2 atmosphere, during 3 months of storage. The gray background indicates a degraded morphology (observed by SEM) while the hatched background delimitates the period when the porous layer begins to morphologically evolve.

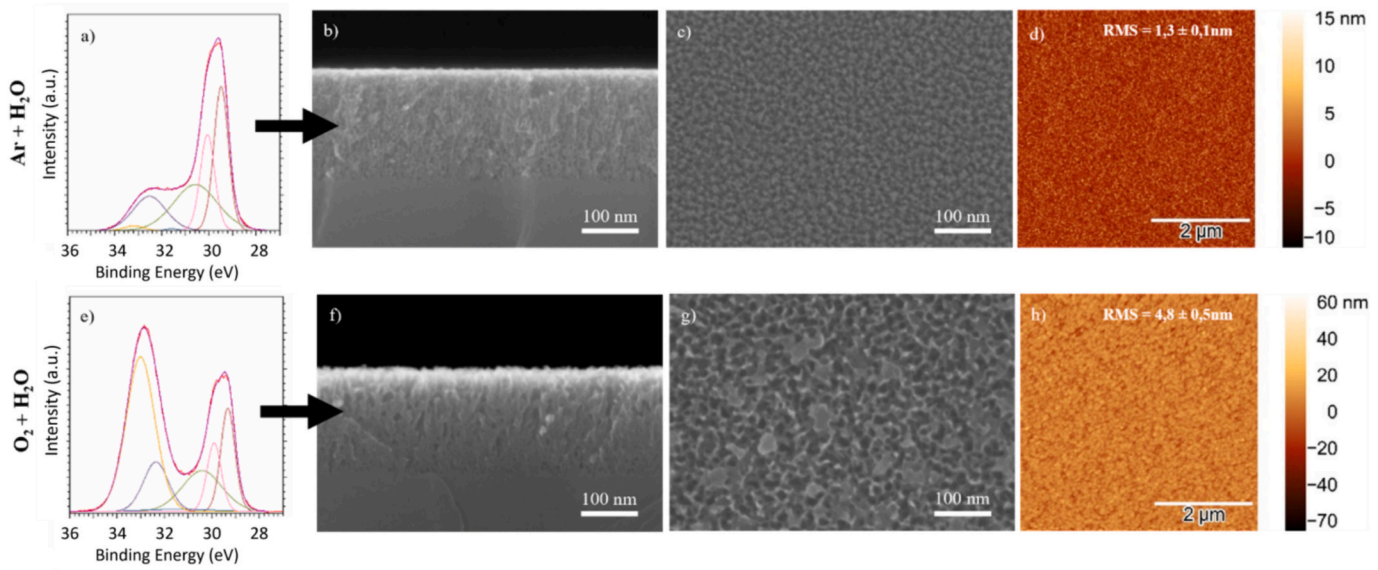

Fig. 8. a) XPS Ge3d spectrum, b) cross-section SEM images, c) Top SEM view and d) 5 × 5um surface roughness made by AFM of porous germanium stored in Ar with humidity. E) XPS Ge3d spectrum, f) cross-section SEM images, g) Top SEM view and h) 5 × 5um surface roughness made by AFM of porous germanium stored in O_2 with humidity, after 3 months of storage.

oxidation and the dissolution of $Ge_{sub\text{-}oxides}$, as proposed in the mechanism illustrated in Fig. 9.

Upon the first exposition of the sample to the $H_2O_{(g)} + O_2$ in the dark (Fig. 9 **(a)**), pores walls are converted into native suboxides (Ge_2O followed by GeO and Ge_2O_3) over the entire depth of the porous structure [18] (Fig. 9 **(b)**). The suboxide layer is then progressively thickened by

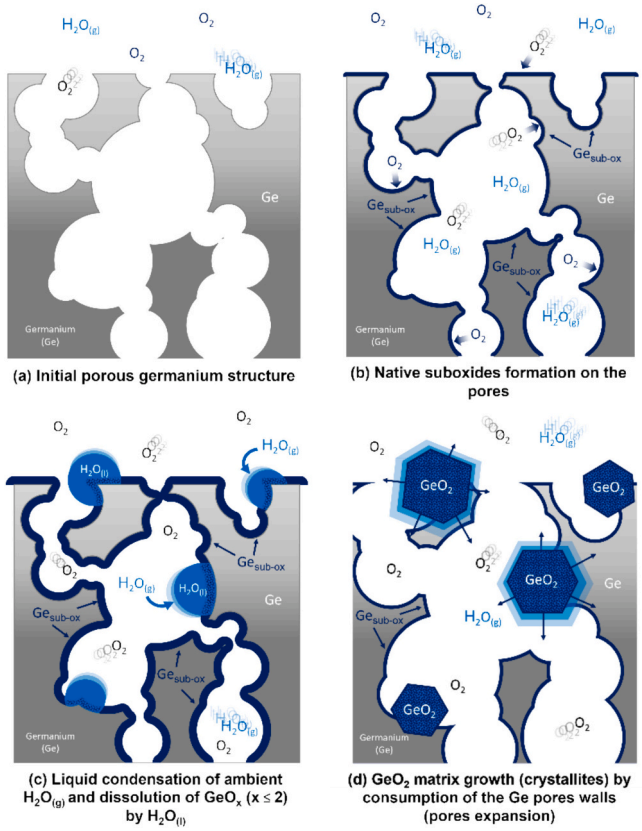

Fig. 9. Schematic illustration of the $Ge_{sub\text{-}oxides}$ layers formation and GeO_2 matrices (clusters) growth mechanism steps in Ge_{porous} structure, under O_2 and Humidity ambient conditions.

the continuous oxidation of the germanium. In parallel, the ambient $H_2O_{(g)}$ and the $H_2O_{(l)}$ accumulated by capillary condensation in the cavities induce local dissolutions of oxides [21,22] by Ge—O bonds hydrolysis [20,23] (Fig. 9 **(c)**). This consumption (etching) of Ge and its oxides by water combined with constant O_2 germanium oxidation continuously forms high oxidation states (Ge^{4+}), which at saturation, precipitate and form visible GeO_2 matrices (Fig. 9 **(d)** and Fig. 8 **(f-g)**).

4.4. *Influence of light*

All the previous characterizations and mechanism descriptions have been based on samples stored inside dark enclosures (dark boxes or hermetic metallic bags). But to clearly understand the role and impact of each ambient parameter, samples exposed to light need also to be characterized. The porous germanium layers in this part are stored in a transparent box with humidity and dioxygen (*light moist O_2*) (under clean room conditions).

4.4.1. *Kinetic: germanium oxide and sub-oxides evolution*

Fig. 10 shows that light exacerbates the oxidation mechanisms of porous germanium. Compared to the storage in similar conditions in the dark (*dark moist O_2*, Fig. 7 **(b)**), the presence of light influences the kinetic of germanium suboxides and oxide formation. The order of oxidation states appearance is similar but faster: after one week, the proportion of GeO_2 (Ge^{4+}) already exceeds 60% and the remaining quantity of germanium Ge^0 falls below 25%. After only 30 days, the quasi-totality of the porous layer has been transformed into GeO_2.

4.4.2. *Morphological evolution after 90 days of storage*

When we pay attention to the morphology of the structure at the end of the aging process (Fig. 11 (a-d)), where the whole germanium has completely evolved into oxide, we only see irregular, and continuous material. The GeO_2 clusters seem to have merged into a compact layer with a surface roughness of 16 ± 1.6 nm, which is not suitable for epitaxial growth. We can also deduce from the comparison with *dark moist O_2* (Fig. 8**(f-g)**) and in *clean room* conditions (Fig. 3**(c-d)**) that the oxidation and morphological transformation are enhanced by the intensity of the light (increase of the energy density brought to the reactions). These SEM and AFM observations correlated to the XPS analysis demonstrate a photo-oxidation of germanium [24] which

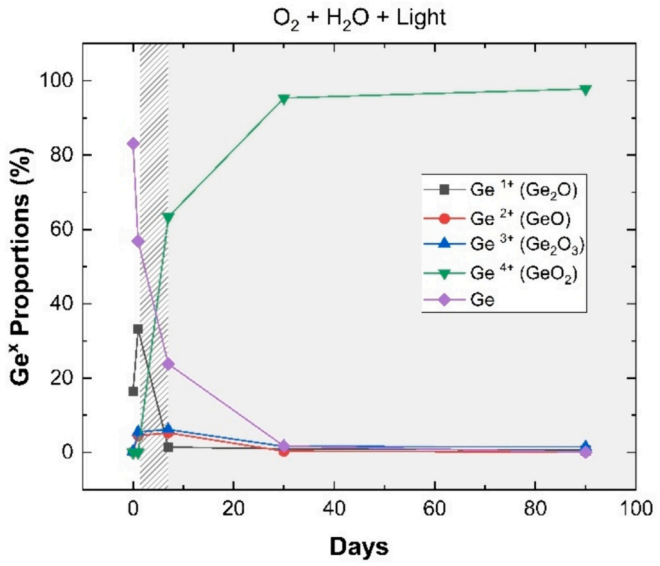

Fig. 10. Proportions of Ge oxides evolution during 90 days under Argon and Oxygen atmosphere with humidity and light with transparent box. The gray background indicates a degraded morphology (observed by SEM) while the hatched background delimitates the period when the porous layer begins to morphologically evolve.

accelerates the structural deterioration of the Ge_{porous}.

4.5. *Reducing porous germanium aging with post-porosification surface treatment*

We have demonstrated that the porous germanium aging results from germanium oxidation, germanium sub-oxide dissolution, and GeO_2 precipitation, and that the suboxide formation seems to be limiting this mechanism in the presence of O_2 and humidity. To delay the aging, we can therefore tailor processes that further reduce the germanium oxidation rate. According to the literature, halogen acids can etch germanium sub-oxides and passivate the surface against oxidation [21,25,26]. *B. Onsia* et al. [21] even showed that HBr and HI remove all the oxides (including suboxides contrary to HF or HCl) and strongly functionalize the Ge surface by Br^- and I^-, respectively, allowing limited passivation and preventing the oxidation over a time that depends on the concentration and the dipping duration in the acids.

To delay the first step of the porous Ge aging mechanism, we applied a wet treatment by dipping a fresh porous germanium sample during 10s in a 1% HBr solution (49% HBr: C_2H_6O (1:198)) before storage. We chose a short dipping time and a low concentration to limit the porous germanium etching that is enhanced by its very high specific surface compared to dense germanium. The sample was then stored in *dark moist* O_2 conditions and its surface composition and morphology evolution with the storage time is compared to untreated samples stored in the same conditions.

4.5.1. *Germanium oxides and sub-oxides evolution*

As shown in Fig. 12 representing the surface composition of the treated porous samples aged during 90 days in *dark moist* O_2 conditions, the high oxidation state quantity has been significantly lowered compared to the untreated sample. During the storage, we observe the same oxidation mechanism with approximately the same proportions of suboxides compared to the samples with no HBr treatment, but at a lower rate. We noticed after 3 months that GeO_2 oxide formation has been limited to under 19% instead of 45% in the untreated sample. These results demonstrate a slowdown of oxidation and prove that the pore's surface passivation by Br can reduce or delay the final formation of Ge^{4+}. This delay in porous germanium oxidation has also been observed (not shown here) for each other storage conditions considered here (*dark dry Ar*, *dark dry* O_2, *dark moist Ar,* and *light moist* O_2).

4.5.2. *Morphological evolution after 90 days of storage*

After 3 months of aging under air condition in the dark (*dark moist* O_2) with initial HBr treatment, the Ge_{porous} layer presents slightly larger porosity (around 68% ± 5%) than the reference sample, a relatively low surface roughness (2.1 ± 0.2 nm) and no visible clusters as shown on Fig. 13 **(b-d)**. These characterizations suggest a continuous etching of the pores during storage and that the creation of clusters is delayed by the initial deoxidation and passivation treatment.

With all the observations of this study (Fig. 14), we can deduce that the visible structural modification happens when the proportion of GeO_2 exceeds a value between 4% and 17% of the total amount of materials (valid with the specific germanium morphology, porosity, and thickness used for these experiments), except when an HBr solution has been applied on the samples before storage. In this condition with a hydrohalogenic acid pretreatment (Fig. 13), we do not observe any cluster appearance despite the presence of large proportions (19%) of GeO_2 oxide compared to the sample stored under a *clean room* environment (Fig. 4). The literature shows that the Ge surface functionalization by halogen atoms such as Br can be removed by water and transformed into HBr (Ge-Br + H_2O = Ge-OH + HBr) [22]. So, we can suppose that HBr is reformed during the dissolution of the walls of the pores suboxides by the $H_2O_{(g)}$ and its liquid condensation ($H_2O_{(l)}$) inside the porous structure (mechanism illustrated in Fig. 9(c)), which then limit the local accumulation GeO_2 due to competition between oxidation O_2 + $H_2O_{(l)}$ and etching by HBr, and thus prevents or delay the clusters formation.

5. Conclusions

Porous germanium is prone to degradation if the storage conditions are inappropriate. Major morphological evolution of monocrystalline mesoporous germanium layers after 90 days of storage under normal clean room environment conditions was investigated by SEM, with an increase of porosity and the formation of clusters. Surface composition

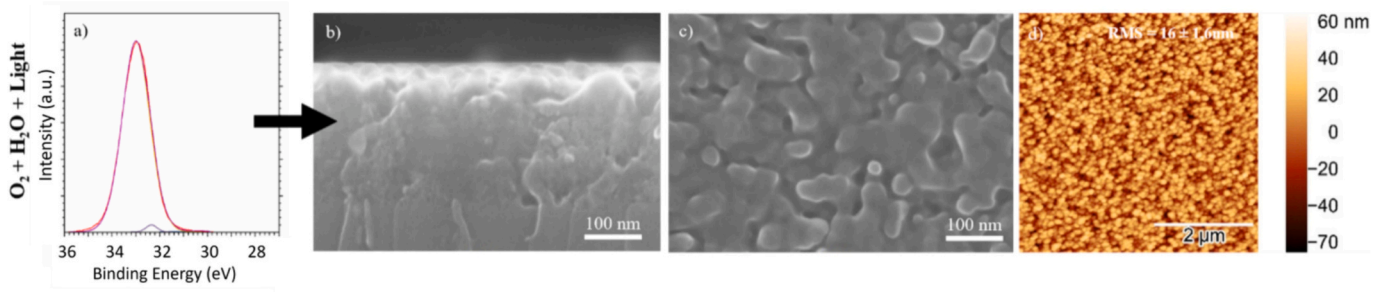

Fig. 11. a) XPS Ge3d spectrum, b) cross-section SEM images, c) Top SEM view and d) 5 × 5um surface roughness made by AFM of porous germanium stored in light moist O_2, after 3 months of storage.

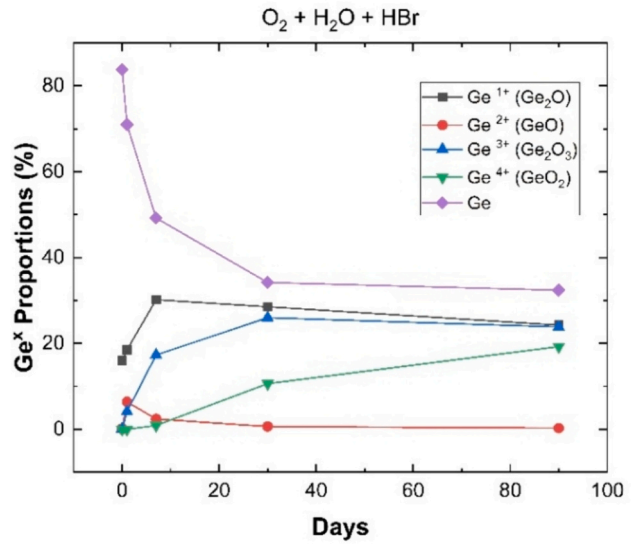

Fig. 12. a) Proportions of Ge oxides evolution during 90 days under Argon and Oxygen atmosphere with humidity and light, with initial HBr treatment before storage (comparable to Fig. 7 (b)).

analysis by XPS demonstrated that the changes in the porous structure are related to the presence of oxides during its aging. Each component of the storage environment was then studied independently and combined to identify precisely the mechanisms responsible for the degradation of the Ge_{porous} layers. Chemical characterizations as a function of time showed that the order of appearance of the Ge suboxides and oxides is always sequenced in the same way: Ge_2O, GeO, Ge_2O_3, and finally GeO_2. The first exposition of the sample to the air induces instantly the formation of a native suboxide layer composed mostly of Ge_2O. After only one day of aging, we also noticed the GeO and Ge_2O_3 creation. Depending on the condition of storage, these suboxides then decrease to give way to GeO_2 oxide. Associated with SEM images of the porous germanium over time, these observations allowed us to conclude that this final oxide GeO_2 is responsible for the cluster formation and the enlargement of the pores by consumption of Ge and suboxides. Concerning the ambient parameters, we saw that ambient dioxygen (O_2) and humidity ($H_2O_{(g)}$) are not individually responsible for GeO_2 production and the related morphological deterioration of the porous structure. This destructive oxidation solely appears when these two storage environmental components are combined. Moreover, when we add light to these aging conditions, we observe an increase in the oxidation effect and faster degradation of the Ge_{porous} layers. This study also highlights that different options are possible to preserve the integrity of germanium samples during storage and increase the shelf life above several months. An encapsulation under a dry neutral atmosphere (Argon) with silicate

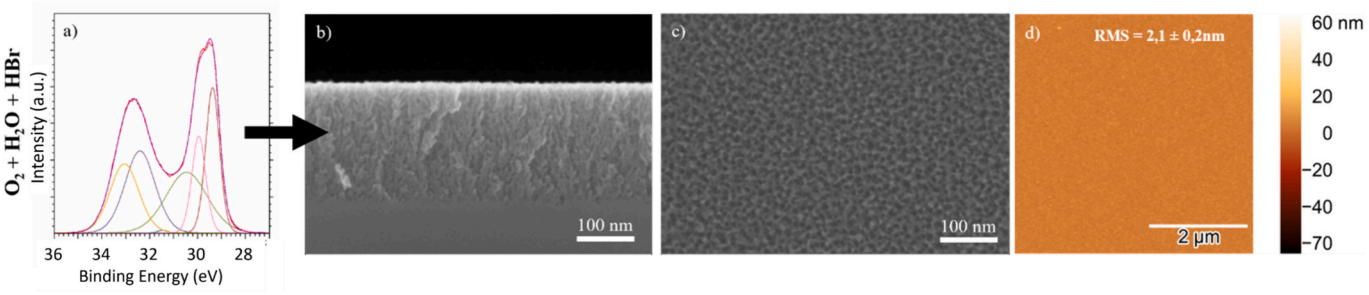

Fig. 13. a) XPS Ge3d spectrum, b) cross-section SEM images, c) Top SEM view and d) 5 × 5um surface roughness made by AFM of porous germanium with initial post-porosification treatment stored in light moist O_2, after 3 months of storage.

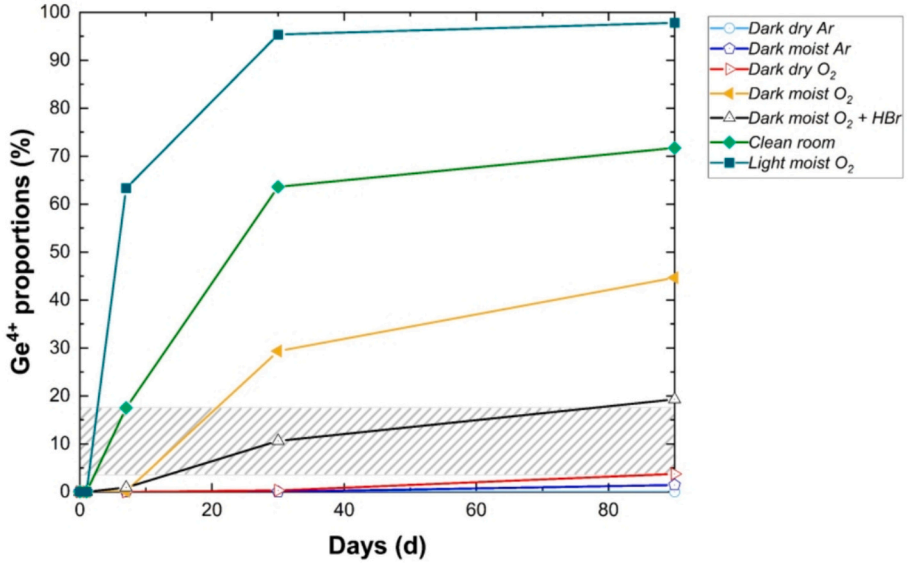

Fig. 14. Comparison of the proportions' evolution of GeO2 oxides (Ge4+) over 90 days for the different conditions studied. The hatched area delimits the period when the porous layer begins to morphologically evolve. Curves with filled points represent the samples that show morphological evolution, while curves with empty points represent the samples that did not change.

beads in hermetic metallic bags or an initial HBr wet treatment is very efficient in reducing or delaying the formation of oxides and thus the potential destruction of the pores. Thanks to these solutions, we can limit the GeO_2 local accumulation that seems to be responsible for the cluster's emergence. These techniques can thus be used to increase the shelf life of porous germanium.

Copyright

Acknowledgment and funding statement

The authors thank Bouraoui Ilahi for the scientific discussions, Alexandre Chapotot for the AFM characterizations, and the 3IT's clean room staff for technical support. The Natural Sciences and Engineering Research Council of Canada (NSERC), Innovation en énergie électrique (InnovÉÉ), Mitacs, and Umicore and Saint-Augustin Canada Electric (Stace) for financial support. LN2 is a joint International Research Laboratory (IRL 3463) funded and co-operated in Canada by Université de Sherbrooke and in France by CNRS as well as ECL, INSA Lyon, and Université Grenoble Alpes (UGA). It is also supported by the Fonds de Recherche du Québec Nature et Technologie (FRQNT). Abderraouf Boucherif is grateful for a Discovery grant supporting this work.

Declaration of competing interest

The authors declare the following financial interests/personal relationships which may be considered as potential competing interests.

Abderraouf Boucherif reports financial support was provided by Umicore. Abderraouf Boucherif reports financial support was provided by InnovÉÉ. Maxime Darnon reports financial support was provided by Natural Sciences and Engineering Research Council of Canada. Maxime Darnon reports financial support was provided by Mitacs Canada. Abderraouf Boucherif reports financial support was provided by Saint-Augustin Canada Electric (Stace). Maxime Darnon reports financial support was provided by Quebec Research Fund Nature and Technology. If there are other authors, they declare that they have no known competing financial interests or personal relationships that could have appeared to influence the work reported in this paper.

Data availability

Data will be made available on request.

References

[1] D.P. Brunco, B. De Jaeger, G. Eneman, A. Satta, V. Terzieva, L. Souriau, F.E. Leys, G. Pourtois, M. Houssa, K. Opsomer, G. Nicholas, M. Meuris, M. Heyns, ECS Trans 11 (2007) 479.
[2] R. Soref, Nat Photonics 4 (2010) 495.
[3] G. Brammertz, Y. Mols, S. Degroote, M. Leys, J. Van Steenbergen, G. Borghs, M. Caymax, J Cryst Growth 297 (2006) 204.
[4] S.P. Tobin, S.M. Vernon, C. Bajgar, V.E. Haven, L.M. Geoffroy, D.R. Lillington, IEEE Electr Dev Lett 9 (1988) 256.
[5] K. Mishra, X.-C. Liu, F.-S. Ke, X.-D. Zhou, Compos Part B Eng 163 (2019) 158.
[6] R. Zegadi, N. Lorrain, L. Bodiou, M. Guendouz, L. Ziet, J. Charrier, J Opt 23 (2021) 035102.
[7] N. Paupy, Z. Oulad Elhmaidi, A. Chapotot, T. Hanuš, J. Arias-Zapata, B. Ilahi, A. Heintz, A.B. Poungoué Mbeunmi, R. Arvinte, M.R. Aziziyan, V. Daniel, G. Hamon, J. Chrétien, F. Zouaghi, A. Ayari, L. Mouchel, J. Henriques, L. Demoulin, T.M. Diallo, P.-O. Provost, H. Pelletier, M. Volatier, R. Kurstjens, J. Cho, G. Courtois, K. Dessein, S. Arcand, C. Dubuc, A. Jaouad, N. Quaegebeur, R. Gosselin, D. Machon, R. Arès, M. Darnon, A. Boucherif, Nanoscale Adv 18 (2023) 4613.
[8] J.P. Toinin, A. Portavoce, K. Hoummada, M. Texier, M. Bertoglio, S. Bernardini, M. Abbarchi, L. Chow, Beilstein J Nanotechnol 6 (2015) 336.
[9] C. Jing, C. Zhang, X. Zang, W. Zhou, W. Bai, T. Lin, J. Chu, Sci Technol Adv Mater 10 (2009) 065001.
[10] H. Yin, W. Xiao, X. Mao, H. Zhu, D. Wang, J Mater Chem A 3 (2015) 1427.
[11] E. Garralaga Rojas, H. Plagwitz, B. Terheiden, J. Hensen, C. Baur, G. La Roche, G.F. X. Strobl, R. Brendel, J Electrochem Soc 156 (2009) D310.
[12] S. Park, J. Simon, K.L. Schulte, A.J. Ptak, J.-S. Wi, D.L. Young, J. Oh, Joule 3 (2019) 1782.
[13] D. Guzmán, M. Cruz, C. Wang, Microelectron J 39 (2008) 523.
[14] T. Hanuš, J. Arias-Zapata, B. Ilahi, P. Provost, J. Cho, K. Dessein, A. Boucherif, Adv Mater Interfaces 10 (2023) 2202495.
[15] V. Daniel, J. Chretien, G. Hamon, M. De Lafontaine, N. Paupy, Z.O. El Hmaidi, B. Ilahi, T. Hanus, M. Darnon, A. Boucherif, 2022 IEEE 49th Photovoltaics Specialists Conference (PVSC), Philadelphia, PA, USA, IEEE, 2022, pp. 0770–0772.
[16] X. Wang, Z. Zhao, J. Xiang, W. Wang, J. Zhang, C. Zhao, T. Ye, Appl Surf Sci 390 (2016) 472.
[17] J. Oh, J.C. Campbell, J Electron Mater 33 (2004) 364.
[18] A.J. Santos, B. Lacroix, F. Maudet, A. Corvisier, F. Paumier, C. Dupeyrat, T. Girardeau, R. García, F.M. Morales, Appl Surf Sci 493 (2019) 807.
[19] S.D. Wolter, T. Tyler, N.M. Jokerst, Thin Solid Films 522 (2012) 217.
[20] K. Prabhakaran, T. Ogino, Surf Sci (1995) 263.
[21] B. Onsia, T. Conard, S. De Gendt, M.M. Heyns, I. Hoflijk, P.W. Mertens, M. Meuris, G. Raskin, S. Sioncke, I. Teerlinck, A. Theuwis, J. Van Steenbergen, C. Vinckier, Solid State Phenom 103–104 (2005) 27.
[22] S. Sun, Y. Sun, Z. Liu, D.-I. Lee, P. Pianetta, Appl Phys Lett 89 (2006) 231925.
[23] M. Jin, O. Veselý, C.J. Heard, M. Kubů, P. Nachtigall, J. Čejka, L. Grajciar, J Phys Chem C 125 (2021) 23744.
[24] S. Sato, S. Nozaki, H. Morisaki, J Appl Phys 81 (1997) 1518.
[25] H. Jagannathan, J. Kim, M. Deal, M. Kelly, Y. Nishi, ECS Trans 3 (2006) 1175.
[26] A. Molina, J.R. Shallenberger, S.E. Mohney, J Vac Sci Technol Vac Surf Films 38 (2020) 023208.